

# From *Rousettus aegyptiacus* (bat) Landing to Robotic Landing: Regulation of CG-CP Distance Using a Nonlinear Closed-Loop Feedback

Usman A. Syed\*, Alireza Ramezani<sup>†</sup>, Soon-Jo Chung<sup>‡</sup>, Seth Hutchinson\*,<sup>†</sup>

**Abstract**—Bats are unique in that they can achieve unrivaled agile maneuvers due to their functionally versatile wing conformations. Among these maneuvers, roosting (landing) has captured attentions because bats perform this acrobatic maneuver with a great composure. This work attempts to reconstruct bat landing maneuvers with a Micro Aerial Vehicle (MAV) called *Alice*. *Alice* is capable of adjusting the position of its Center of Gravity (CG) with respect to the Center of Pressure (CP) using a nonlinear closed-loop feedback. This nonlinear control law, which is based on the method of input-output feedback linearization, enables attitude regulations through variations in CG-CP distance. To design the model-based nonlinear controller, the Newton-Euler dynamic model of the robot is considered, in which the aerodynamic coefficients of lift and drag are obtained experimentally. The performance of the proposed control architecture is validated by conducting several experiments.

## I. INTRODUCTION

Nature has always been a source of inspiration for the design and control of smart machines [1],[2],[3],[4]. The area of bio-inspired robotics has been actively pursued, both to understand nature as well as to mimic nature's optimal creations.

Bio-inspired robots have been built to understand the use of inertial appendages by animals in the control of their locomotion [5]. Among animals, bats are known to use the inertia of appendages such as arms, legs, and tails to perform a wide variety of agile maneuvers. They have the most sophisticated powered flight mechanism among animals. This flight apparatus possesses many joints, which couple the muscles and bones to each other and synthesizes a versatile dynamic conforming musculoskeletal system that has 40 Degrees of Freedom (DoFs) [6]. Some of these joints are active and some are passive. Because of these dynamic wing conformations, bat's are able to perform agile maneuvers such as turning sharply, landing, etc.

Roosting (landing) involves the harmonious movement of bats' several joints and muscles. Recent analysis of *Rousettus aegyptiacus* landing utilizing on-board inertial measurement sensors and off-board high-speed imaging techniques [7] suggests that the landing maneuver takes place in the sagittal

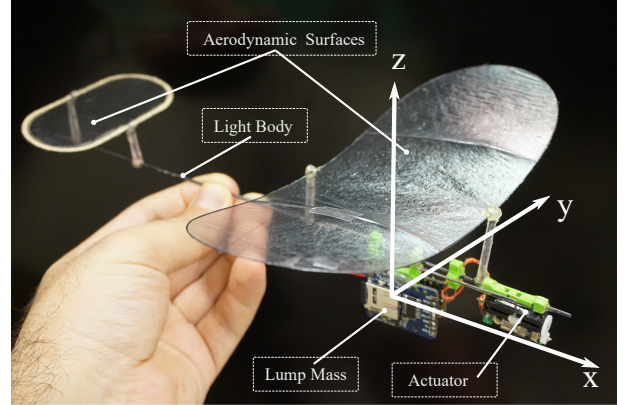


Fig. 1: *Alice* is a 1-DoF robotic platform that is used to validate the landing model of a biological bat introduced in [7].

plane<sup>1</sup> and it involves joint movements at shoulder, elbow, and wrist. The collective outcome of such joint movements regulates the pitching moment required for landing by varying the distance between Center of Gravity (CG) and Center of Pressure (CP). In [7] authors present a landing model of a biological bat and compares the flight data from this model with the flight data from biological bats. This comparison confirms that bats indeed manipulate their CP-CG distance for their pitch control while landing.

In this work, we aim at reproducing the agile maneuvers that are demonstrated by bats while landing. In particular, we are motivated by reconstructing the landing maneuver of *Rousettus aegyptiacus* utilizing our biologically inspired bat robot, which is called Bat Bot (B2) [8], [9]. Recent observations of the landing in *Rousettus aegyptiacus* suggest that the landing maneuver involves mainly the longitudinal dynamics. In other words, it occurs in the sagittal plane of flight. They initiate the landing maneuver by sweeping the wings and regulating a pitch-up movements. Then, once in proximity of the landing surface, they proceed by moving the legs ventrally and grabbing the landing surface.

Motivated by the landing maneuver, this work aims at two objectives. First, validating the effectiveness of CG-CP distance regulations to achieve maneuverable and agile flights, in particular high-angle pitch-up maneuver. Second,

\* Authors are with Department of Electrical and Computer Engineering, University of Illinois, Urbana, IL, 61801 usyed3@illinois.edu, seth@illinois.edu

<sup>†</sup>Authors are with Coordinated Science Laboratory (CSL), University of Illinois, Urbana, IL, 61801 aramez@illinois.edu

<sup>‡</sup>Author is with Graduate Aerospace Laboratory, California Institute of Technology, Pasadena, CA, 91125 sjchung@caltech.edu

<sup>1</sup>Sagittal plane is an anatomical plane that divides a body into its left and right halves.

increasing the performance of CG-CP regulations by employing a model-based nonlinear controller.

We employed a MAV called *Alice* for these objectives. *Alice* possesses a light frame and a lump of mass that moves with respect to the body frame. Since the lump of mass consists a major part of the total weight of the system, displacing the mass yields variations in the CG-CP distance.

In addition, *Alice* possesses on-board electronics including a microprocessor, an Inertial Measurement Unit (IMU) and a linear servo actuator. These on-board electronics make it possible to embed a controller in the system and close the feedback loop by reading the attitude of the system and regulating the CG-CP distance. The rest of this section highlight similar strategies employed by animals for their attitude control and related research in the field of robotics.

#### A. Attitude Control in Biological Systems

Bats are not the only animals that perform attitude adjustments through movements of lump mass. Early studies on flying locusts [10] have shown that locusts use their abdomens as rudders in their flight control. Locusts also use lateral deflections of abdomen in yaw correction [11]. Wind receptor hairs on locusts control the vertical position of abdomen in relation to variations of wind speed while changes in wind direction stimulate yaw corrections.

The movements of a lump of mass yields variations in the momentum in the system. Lizards use this technique to adjust their body orientation as tail movements in lizards act like a dynamic stabilizer for pitch control [12]. Lizards swing their tails in the sagittal plane so as to redirect angular momentum from their bodies to their tails, leading to the pitch control of their bodies. In an attempt to understand tail use for control, a lizard-sized robot have been developed to investigate the effectiveness of tails in attitude control [12]. A comparative study of tail effectiveness in the attitude control for biological lizards and lizard-size tailed robots is presented in [12], [13]. Utilizing contact forces and zero angular momentum condition, the lizard-inspired robot uses a Proportional-Derivative (PD) controller for self-righting in a free fall. The attitude controller for the robot with 2-DOF tail has been presented in [14].

Arboreal animals also utilize inertial appangates. Often they fall out of trees as a result of uneven terrain, predator-prey conditions or fighting behavior. During their ballistic fall they are capable of self-righting in mid-air, thereby avoiding injuries, e.g., air righting behavior in flat-tailed house geckos [15]. Appendage inertia in geckos has a vital role in arboreal acrobatics performance such as climbing, aerial descent, and gliding. By conserving the angular momentum, geckos can self-right themselves in mid-air (using their tails) to achieve a gliding posture. While in gliding motion, they can yaw by further swinging their tails. Posture control in free fall has also been reported in other animals. Rats are reported to perform a spiral movement using head-torso and torso-pelvis rotations for self righting in mid-air [16]. Righting with the tail alone has not yet been found in such animals.

Other than geckos and rats, cats also perform self-righting to land on their feet. Cats perform the righting maneuver by rotating while maintaining the condition of zero total angular momentum. Cats change their shape by bending their bodies in mid-air, which forces their bodies to rotate in the opposite direction while maintaining the zero angular momentum condition [17].

Insects utilize CG adjustments as well. Recent work [18] has investigated the role of visual-abdominal reflexes in Hawkmoth in regards to the flight control problem. It has been demonstrated that Hawkmoths actively uses the angular position of thoracic-abdominal joint in its hovering flight. Hawkmoths articulate their abdomens to redirect the lift force generated by their wings to maintain a stable hovering flight. Fruit flies also change their CG during flight by changing the posture of their abdomens with respect to the plane of wing oscillation [19]. In fruit flies, the abdomen behaves as a rudder for rotation control about transversal<sup>2</sup> body axis.

#### B. Attitude Control in Robotics Research

The idea of manipulating system's CG have been widely employed in the biologically inspired robots. For instance, this method has been extensively explored in the field of atmospheric reentry vessels, underwater vehicles and aerial robotics. *muFR* [20] and *CoaX* [21] are two helicopters that control their attitude by actuating a significant part of their mass and thereby modifying their CG. *muFR* moves its battery in a plane to manipulate its CG, while *CoaX* moves its battery on a spherical surface to change its CG. PD controllers are used for the attitude control of *CoaX* while *muFR* use a PID control law.

Similar to aerial robots, moving mass control is extensively utilized in remotely operated Autonomous Underwater Vehicles (AUVs). One such example is an Eyeball Remotely Operated Vehicle (ROV) [22]. It can reorient using an internal eccentric mass and uses a proportional controller with linearized system dynamics for pitch and velocity control. Similarly, [23] has investigated the control of an AUV in a vertical plane using a thruster and a point movable mass using a back stepping control policy for tracking desired trajectories. And [24] has employed linear quadratic regulators to control underwater gliders wherein internal mass redistribution is utilized for attitude control of a buoyancy-propelled, fixed wing glider. Directly altering the angular momentum by using internal rotors is similar to the idea of CG change, which is often used to stabilize AUVs. For instance, [25] designed a Lyapunov based dissipative feedback control law that stabilizes the system dynamics by reshaping the kinetic energy of the conservative system dynamics. In comparison to these robotic systems, in addition to the simulated results, this work experimentally validates the nonlinear controller, which the aforementioned robotic systems lack.

This work is organized as follows. An overview of *Alice* and its avionics is presented in Section II. In Section III a

<sup>2</sup>Transversal body axis is the body pitch axis.

nonlinear model of *Alice* is derived and its system identification is discussed. Using this model, a nonlinear control law for tracking a reference pitch trajectory is derived in Section IV. Preliminary experimental flight results are presented and compared with simulation in Section V. Conclusion and future work are given in section VI.

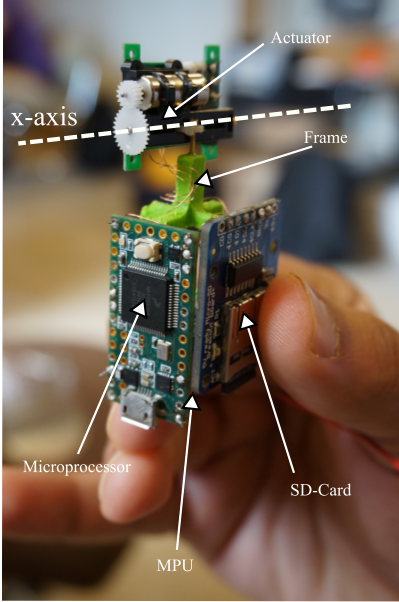


Fig. 2: *Alice*'s avionics and actuation mechanism.

## II. ALLICE: SYSTEM OVERVIEW

*Alice* (shown in Fig. 1) is a miniature fixed-wing MAV that has been modified to adjust its CG-CP distance. It utilizes variations in CG-CP distance as an effective control strategy for the attitude control of the overall system. *Alice* has conventional aerodynamic surfaces, including a fixed-wing and a tail. In order to regulate the aerodynamic moments around CG, instead of displacing these conventional control surfaces, a moving mass (shown in Fig. 2), which measures 56% of the total mass of the system, is translated along the body x-axis (are shown in Fig. 1 and Fig. 2). Since the lump mass is a major part of the total mass, the adjustments in CG positions with respect to the airframe yields variations in CG-CP distance.

*Alice* is equipped with on-board electronics (shown in Fig. 2) including: 1) a 32 bit ARM Cortex M4 microprocessor having a 64K RAM equipped with serial communication capabilities including Inter-Integrated Circuit (I2C) and Serial Peripheral Interface (SPI), 2) a 9-axis Inertial Measurement Unit (IMU), MPU-9250. MPU-9250 has a 3-axis gyro, 3-axis accelerometer and a 3-axis digital compass. It is also equipped with an on-board Digital Motion Processor, 3) a MicroSD card reader/writer, 4) a 900MHz RC receiver for controlling MAV's propeller speed, and 5) a micro linear servo capable of moving the lump of mass in either direction.

The inertial measurements are read at 60 Hz, and nonlinear control is also executed in real-time at 60 Hz ; data recording on the SD-Card occurs at 30 Hz. IMU is interfaced with the

microprocessor using  $I^2C$  communication interface while the SPI communication protocol is used for data storage on the SD-card.

The physical parameters of the aircraft are listed in Table I.

## III. NONLINEAR DYNAMIC MODEL

*Alice* is modeled using the method of Newton-Euler. The nonlinear model consists of twelve states: six translational and six angular states. A Cartesian body coordinate frame is considered at MAV's CG (without considering the lump mass) with  $\mathbf{x}$ -axis pointing forward and  $\mathbf{z}$ -axis pointing upwards. The translational state variables are the position and velocity of CG with respect to a fixed inertial (world) coordinate frame; they are denoted by  $\mathbf{p} = (p_x; p_y; p_z)$  and  $\mathbf{v} = (\dot{p}_x; \dot{p}_y; \dot{p}_z)$ .

The angular states are defined as the attitude of the body axis with respect to the inertial frame and the body axis angular velocity. The former is denoted by  $\mathbf{q} = (q_x; q_y; q_z)$  where  $q_x$ ,  $q_y$ , and  $q_z$  are the roll, pitch, and yaw angles, respectively; the latter is denoted by  $\boldsymbol{\omega} = (\omega_x; \omega_y; \omega_z)$  where  $\omega_x$ ,  $\omega_y$ , and  $\omega_z$  are the body axis angular velocity. As a result, the state vector is given by

$$\mathbf{x} = (\mathbf{p}; \mathbf{q}; \mathbf{v}; \boldsymbol{\omega}). \quad (1)$$

The input to the system are the position of the lump of mass (shown in Fig. 1) along body axes, with respect to MAV's CG. Here, it is assumed that the aerodynamic forces, including the lift and drag force, act on CP of the wing and tail. CP is located at the quarter chord point [26].

### A. Kinematics

The rotation matrix  $\mathcal{R}_b^i(\mathbf{q})$  maps the body coordinate vectors to the world coordinate vectors. The rotation matrix is computed using **ZYX** Euler convention [27].

The wing has an incidence angle  $\theta_w$ , and dihedral angles of  $\delta_R$  and  $\delta_L$  for the right and left parts, respectively. The tail structure has an incidence angle  $\theta_t$  without any dihedral angle. Given these predefined incidence and dihedral angles, the rotation transformations from the wing and tail coordinate frames to the body coordinate frame are given by  $\mathcal{R}_w^b(\theta_w, \delta)$  and  $\mathcal{R}_t^b(\theta_t)$ , respectively. These rotation matrices are used in the subsequent subsection to transform the velocities and aerodynamic forces from the wing and tail coordinate frames to the body coordinate frame.

Parameter	Value
Aircraft Mass	23.15 g
Wing span	19.5 cm
Wing chord	7.7 cm
$I_{xx}$	$11.95 \times 10^{-5}$ kg m
$I_{yy}$	$2.60 \times 10^{-3}$ kg m
$I_{zz}$	$3.91 \times 10^{-5}$ kg m
$I_{xz}$	$5.25 \times 10^{-5}$ kg m
$\theta_w$	$6^\circ$
$\theta_t$	$-7.5^\circ$
$\delta_R, \delta_L$	$12^\circ$

TABLE I: Physical parameters of *Alice*.

The inertial position  $\mathbf{p}$  and velocity  $\mathbf{v}$  of CG are related by

$$\dot{\mathbf{p}} = \mathbf{v}. \quad (2)$$

The Euler angles  $\mathbf{q}$  and the body angular rates  $\boldsymbol{\omega}$  are related by

$$\dot{\mathbf{q}} = \begin{pmatrix} 1 & S_x \frac{S_y}{C_y} & C_x \frac{S_y}{C_y} \\ 0 & C_x & S_x \\ 0 & \frac{S_x}{C_y} & \frac{C_x}{C_y} \end{pmatrix} \boldsymbol{\omega}. \quad (3)$$

### B. Equations of motion

The aerodynamic and weight forces are the only forces that act on the system. The aerodynamic forces are computed using strip theory [28]. Strip theory suggests that the aerodynamic surface of the wing and tail can be divided into small chord-wise strips, and the collective sum of the forces and moments that act on each strip would reflect the overall force and moment. The force and moment acting on each strip can be computed using a suitable aerodynamic model [29]. In this paper, it is assumed that the lift  $F_L$  (orthogonal to the local velocity) and drag  $F_D$  (parallel with the local velocity) forces act on the wing or tail CP, which is located quarter-chord behind the leading edge [26]. They are given by

$$F_L = \bar{q} A C_L \quad (4)$$

$$F_D = \bar{q} A C_D \quad (5)$$

where  $A$  represents the surface area of the wing and tail;  $C_L$  and  $C_D$  are the coefficient of lift and drag;  $\bar{q} = \rho \frac{V_{CP}^2}{2}$  is the dynamic pressure, where,  $\rho$  is air density and  $V_{CP}$  is the local velocity at CP. Here, the aerodynamic force and moment on fuselage are not considered as the fuselage is made of slender carbon-fiber rods, which has a negligible aerodynamic resistance.

The aerodynamic coefficients are functions of angle of attack  $\alpha$  and are given by

$$\begin{aligned} C_L &= C_{L0} + C_{L\alpha} \alpha, \\ C_D &= C_{D0} + C_{D\alpha} \alpha + C_{D\alpha^2} \alpha^2. \end{aligned} \quad (6)$$

where  $C_{L0}$  is the lift coefficient at zero angle of attack,  $C_{L\alpha}$  is the lift slope given by  $\frac{\partial C_L}{\partial \alpha} \big|_{\alpha=0}$ ,  $C_{D0}$  is the drag coefficient at zero angle of attack,  $C_{D\alpha}$  and  $C_{D\alpha^2}$  are first and second order drag slopes given by  $\frac{\partial C_D}{\partial \alpha} \big|_{\alpha=0}$  and  $\frac{\partial^2 C_D}{\partial \alpha^2} \big|_{\alpha=0}$ . The overall force produced by wings (likewise force from tail can also be determined in a similar manner), defined in the body coordinate frame are given by

$$\begin{pmatrix} X_w \\ Y_w \\ Z_w \end{pmatrix} = \sum_{i=1}^n \mathcal{R}_w^b \begin{pmatrix} F_{Li} \sin \alpha_i - F_{Di} \cos \alpha_i \\ 0 \\ -F_{Li} \cos \alpha_i - F_{Di} \sin \alpha_i \end{pmatrix} \quad (7)$$

where  $n$  is the total number of strips.

The Newton's equations of motion are written in the inertial frame and are given by

$$\dot{\mathbf{v}} = \frac{1}{m} \mathcal{R}_b^i \left( \begin{pmatrix} X_w \\ Y_w \\ Z_w \end{pmatrix} + \begin{pmatrix} X_t \\ Y_t \\ Z_t \end{pmatrix} + \begin{pmatrix} X_T \\ 0 \\ 0 \end{pmatrix} \right) - \begin{pmatrix} 0 \\ 0 \\ g \end{pmatrix} \quad (8)$$

where  $X_T$  is a constant thrust force acting along the body  $\mathbf{x}$ -axis and reflects the presence of the propeller in front of the MAV;  $w$  and  $t$  subscripts denote the wing and tail forces, respectively;  $m$  and  $g$  are the total mass and gravity constant. Turning to the moments generated by aerodynamic forces around CG, as reported by [29], the body axis moment generated by the aerodynamic force on the wings is given as follows:

$$\begin{pmatrix} L_w \\ M_w \\ N_w \end{pmatrix} = \bar{q} A \begin{pmatrix} C_{l\bar{c}} \\ C_{m\bar{c}} \\ C_{n\bar{c}} \end{pmatrix} \quad (9)$$

where  $\bar{c}$  and  $b$  are the mean aerodynamic chord and span of the wing, respectively;  $C_l$ ,  $C_m$ , and  $C_n$  are given by

$$\begin{aligned} C_l &= C_{l0} + C_{l\beta} \beta + C_{l\hat{p}} \hat{p} + C_{l\hat{r}} \hat{r} \\ C_m &= C_{m0} + C_{m\alpha} \alpha + C_{m\hat{q}} \hat{q} \\ C_n &= C_{n0} + C_{n\beta} \beta + C_{n\hat{p}} \hat{p} + C_{n\hat{r}} \hat{r} \end{aligned} \quad (10)$$

where  $\beta$  is the side slip angle;  $\hat{p}$ ,  $\hat{q}$  and  $\hat{r}$  are normalized roll, pitch and yaw rate angles.  $C_{m0}$  is pitching moment coefficient at zero angle of attack;  $C_{l0}$  and  $C_{n0}$  are roll and yaw moment coefficients for zero side slip angle.  $C_{l\beta}$ ,  $C_{m\alpha}$  and  $C_{n\beta}$  are moment slopes given by  $\frac{\partial C_l}{\partial \beta} \big|_{\beta=0}$ ,

$\frac{\partial C_m}{\partial \alpha} \big|_{\alpha=0}$  and  $\frac{\partial C_n}{\partial \beta} \big|_{\beta=0}$  respectively. Other terms including  $C_{l\hat{p}}$ ,  $C_{l\hat{r}}$ ,  $C_{m\hat{q}}$ ,  $C_{n\hat{p}}$  and  $C_{n\hat{r}}$  reflect the contribution of the angular velocity to the body axis moments.

Now, the Euler equations of motion are given by

$$\dot{\boldsymbol{\omega}} = \mathbf{I}^{-1} (\mathbf{M} - \mathbf{S}(\boldsymbol{\omega}) \mathbf{I} \boldsymbol{\omega}) \quad (11)$$

where

$$\mathbf{M} = \begin{pmatrix} L_w \\ M_w \\ N_w \end{pmatrix} + \begin{pmatrix} L_t \\ M_t \\ N_t \end{pmatrix} \quad (12)$$

is the moment generated by the wing and tail aerodynamic forces around CG,  $\mathbf{I}$  is the inertia tensor defined in the body coordinate frame and  $\mathbf{S}(\boldsymbol{\omega})$  is the skew symmetric matrix representation of the angular velocity  $\boldsymbol{\omega}$ .

The nonlinear dynamic model of *Allice* is thus given by (2), (3), (8) and (11). The system of nonlinear equations is denoted by

$$\dot{\mathbf{x}} = \mathbf{f}(\mathbf{x}). \quad (13)$$

### C. Longitudinal Dynamics

Lateral and transversal dynamics have negligible contributions in the landing maneuver of bats [7]. As a result, the nonlinear system given by (13) is augmented with the constraint equations given by

$$\mathbf{G}(\mathbf{x}) : \begin{cases} p_y = 0, \\ v_y = 0, \\ q_{x,z} = 0, \\ \dot{q}_{x,z} = 0. \end{cases} \quad (14)$$

Free body diagram of the constrained system is presented in Fig. 3. The constrained dynamics represents the longitudinal dynamics and will be employed as follows.

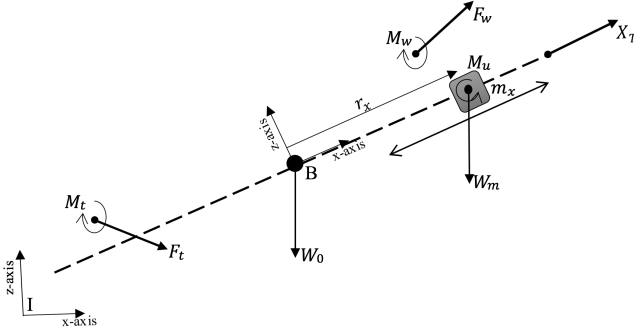


Fig. 3: Free body diagram of constrained system.

Here, the control action  $u$  is considered as of the position of the moving lump of mass  $m_x$  along  $x$ -axis, which is used to manipulate CG-CP distance. The position vector of the moving mass in the body coordinate frame is given by  $\mathbf{r}_x = (u; 0; 0)$ . Consequently, the generated moment around CG is given by

$$\begin{pmatrix} L_u \\ M_u \\ N_u \end{pmatrix} = S(\mathbf{r}_x) \mathcal{R}_i^b \begin{pmatrix} 0 \\ 0 \\ m_x g \end{pmatrix} = \kappa(\mathbf{x})u. \quad (15)$$

Now, considering the nonlinear dynamic model (13), the constraint equations(14) and moving mass moment (15), the longitudinal nonlinear dynamic model of *Alice* is an affine-in-control dynamics given by

$$\dot{\mathbf{x}} = f_{con}(\mathbf{x}) + g(\mathbf{x})u \quad (16)$$

where the subscript "con" denotes the term "constraint" and  $g(\mathbf{x}) = \mathbf{I}^{-1} \kappa(\mathbf{x})$ .

#### D. System Identification

The unknown parameters, such as the inertia tensor  $\mathbf{I}$  (see Table I) and the aerodynamic coefficients (see Table II), were obtained experimentally.

The inertia tensor of a MAV is experimentally determined with a swing test [30]. A swing test for each axis is carried out by swinging the body about individual axes like a pendulum. A compound pendulum setup is used for determining  $I_{xx}$ ,  $I_{yy}$  and  $I_{xz}$  while a bifilar pendulum configuration is used for determining the inertia about yaw axis  $I_{zz}$ .

Then, the aerodynamic coefficients were obtained by comparing the simulated state trajectories of the system with experiments. First, the flight data were recorded for ten flights using the on-board sensors and electronics. Then, the data for each flight was normalized to a unit time interval. Time normalized flight data of ten flights was then used to obtain the median flight and the confidence bounds (max and min limits of flight states) associated with each state trajectory. A nonlinear and finite-state optimization problem helped finding the coefficients by minimizing the

performance index given by

$$\mathcal{J} = \frac{1}{2} \int_0^{t_f} (q_y - \hat{q}_y)^2 + (\omega_y - \hat{\omega}_y)^2 + (v_x - \hat{v}_x)^2 + (v_z - \hat{v}_z)^2 dt. \quad (17)$$

where  $t_f$  is the flight time envelope;  $\hat{q}_y$ ,  $\hat{\omega}_y$ ,  $\hat{v}_x$  and  $\hat{v}_z$  are the observed quantities from the flight data. Table II shows the estimated values, and Fig. 4 depicts the agreement between the simulated trajectories, which are computed using the estimated coefficients and experiments.

#### IV. NONLINEAR CONTROL LAW

In this work a nonlinear feedback controller based on the method of feedback linearization is applied to steer the system given by (16). The idea is to cancel the nonlinearity (e.g., aerodynamic terms) in the system. In general, nonlinearity cancellation does not apply to every nonlinear system and requires class of systems that are affine-in-control. Unfortunately, MAVs with conventional steering control surfaces such as elevator, rudder, etc., fall in the category of non-affine-in-control nonlinear systems [31] because the control action (e.g., the position and velocity of the elevator) appears implicitly inside the aerodynamic forces and moments. Our choice of control input (CG displacement) yields a system that is affine-in-control where rules of nonlinear control theory are applicable. Now the feedback design follows.

We initiate with two basic definitions of the relative degree  $r$  and feedback linearization.

**Definition 4.1.** [32] *The nonlinear system given by (16) and an output function  $y = h(x)$  has a relative degree  $1 \leq r \leq n$  in a region  $D_0 \subset \mathbb{R}^n$  if for all  $x \in D_0$*

$$L_g L_f^{i-1} h(x) = 0 \quad i = 1, 2, 3, \dots, r-1; L_g L_f^{r-1} h(x) \neq 0 \quad (18)$$

In the definition above, the Lie derivative of a vector field  $h(x)$  along the vector field  $f(x)$  is given by

$$L_f h(x) = \frac{\partial h(x)}{\partial x} f(x), \quad (19)$$

and higher order Lie derivatives are recursively given by

$$L_f^k h(x) = \frac{\partial L_f^{k-1} h(x)}{\partial x} f(x). \quad (20)$$

**Definition 4.2.** [32] *The nonlinear system given by (16) and the output function  $y = h(x)$  with sufficiently smooth vector fields  $f_{con}(x)$  and  $g(x)$  on a domain  $D \subset \mathbb{R}^n$  is*

Parameter	Estimated Value
$C_{L0}$	129.44
$C_{L\alpha}$	-76.81
$C_{D0}$	-42.69
$C_{D\alpha}$	-14.21
$C_{D\alpha^2}$	53.58
$C_{m0}$	121.18
$C_{m\alpha}$	-309.33
$C_{m\dot{q}}$	-736.82

TABLE II: Estimated aerodynamic coefficients.



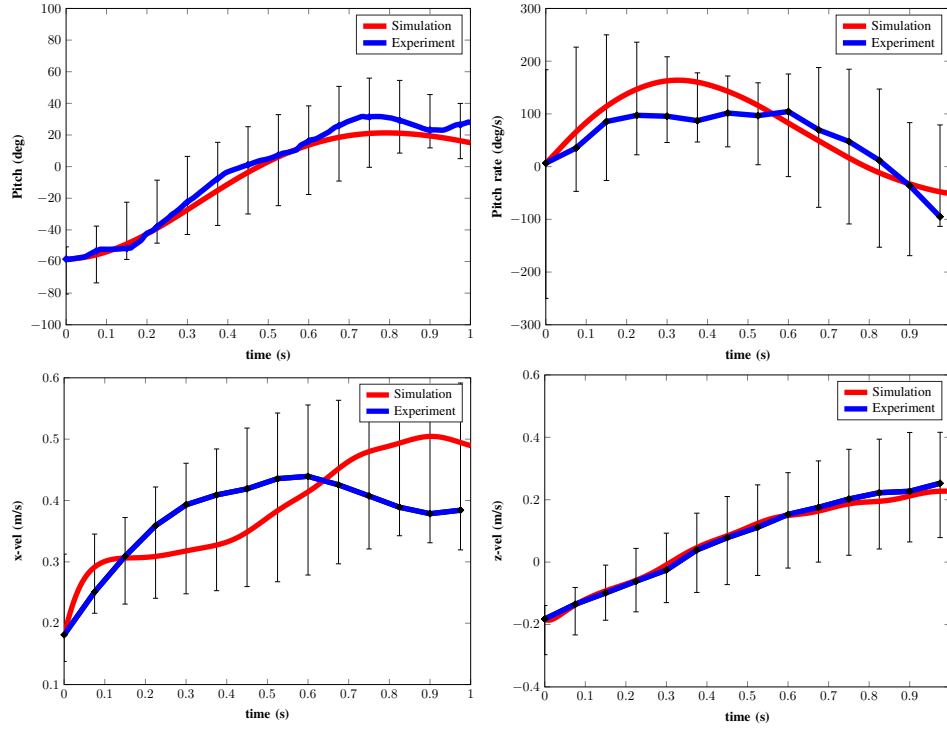


Fig. 4: A comparison between the simulated trajectories and experiments; the estimated aerodynamic coefficients (Table II) have been employed to compute the simulated trajectories.

said to be partially feedback linearizable if there exists a diffeomorphism  $T : D \rightarrow \mathbb{R}^n$  that contains the origin and the change of variables  $z = (\eta; \xi) = T(x)$  transforms the system (16) into two subsystems given by

$$\begin{aligned} \dot{\eta} &= f_0(\eta, \xi) \\ \dot{\xi} &= A\xi + B\gamma(x)(u - \alpha(x)) \end{aligned} \quad (21)$$

where  $\xi \in \mathbb{R}^r$  the feedback linearizable subsystem and  $\eta \in \mathbb{R}^{n-r}$  the internal dynamics;  $(A, B)$  is controllable;  $\gamma(x)$  is nonsingular for all  $x \in D$ ;  $f_0(0, 0) = 0$ ;  $f_0(\eta, \xi)$ ,  $\alpha(x)$  and  $\gamma(x)$  are continuously differentiable.

Since on a system with relative degree  $r$

$$y^{(r)} = L_f^r h(x) + L_g L_f^{r-1} h(x) u, \quad (22)$$

therefore it is straightforward to verify that the nonlinear feedback law given by

$$u = \left( L_g L_f^{r-1} h(x) \right)^{-1} (v - L_f^r h(x)) \quad (23)$$

will reduce the closed-loop system to

$$y^{(r)} = v \quad (24)$$

which is a cascade of  $r$  integrators and can be stabilized by choosing suitable  $v$ . Lets choose the output function

$$y = q_y - q_d(t) \quad (25)$$

where  $q_d(t)$  is a desired pitch angle command. We use the feedback design scheme explained above to set the output function equal to zero. This implies the pitch angle regulation

or tracking. By taking the time derivatives of the output function it is easy to observe that the relative degree  $r = 2$ . As a result the system is partial feedback linearizable. The feedback linearizable subsystem  $\xi$  is given by

$$\begin{pmatrix} \dot{\xi}_1 \\ \dot{\xi}_2 \end{pmatrix} = \begin{pmatrix} \dot{q}_y - \dot{q}_d(t) \\ \mathbf{I}^{-1} (M + \kappa(x)u) \end{pmatrix} \quad (26)$$

The decoupling matrix given by

$$\gamma(x) = \mathbf{I}^{-1} \kappa(x) \quad (27)$$

is nonsingular for the entire state space except when the MAV is pitched at 90 degrees.

Now, the control input given by (23) renders the feedback linearizable subsystem stable. In other words, the system tracks the desired pitch angle trajectory  $q_d(t)$ . Following (23), the control input is given by

$$u = \left( \mathbf{I}^{-1} \kappa(x) \right)^{-1} (v - M) \quad (28)$$

where  $v = -k_p(q_y - q_d) - k_d(\dot{q}_y - \dot{q}_d)$ ;  $k_p$  and  $k_d$  are controller gains.

## V. RESULTS

The Control law designed in the last section was tested for numerous reference trajectories. The methodology adopted for reporting performance of the controller is based on the statistical properties of the flight data. Experiments were conducted by throwing *Alice* in air with the propeller activated at its maximum speed. A safety net was employed to avoid any damage to the MAV. In all the experiments, the

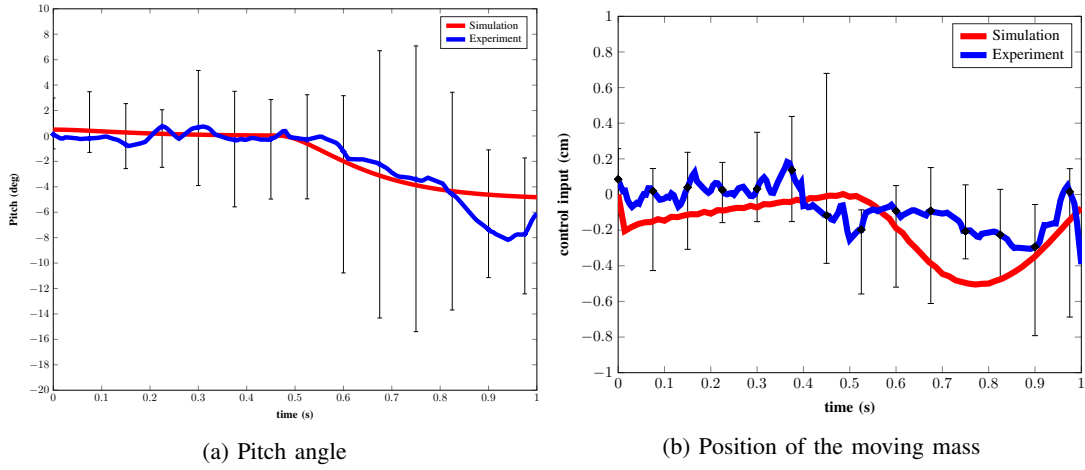


Fig. 5: A comparison of the simulated and experimental trajectories with  $5^\circ$  pitch up (negative) as a desired reference.

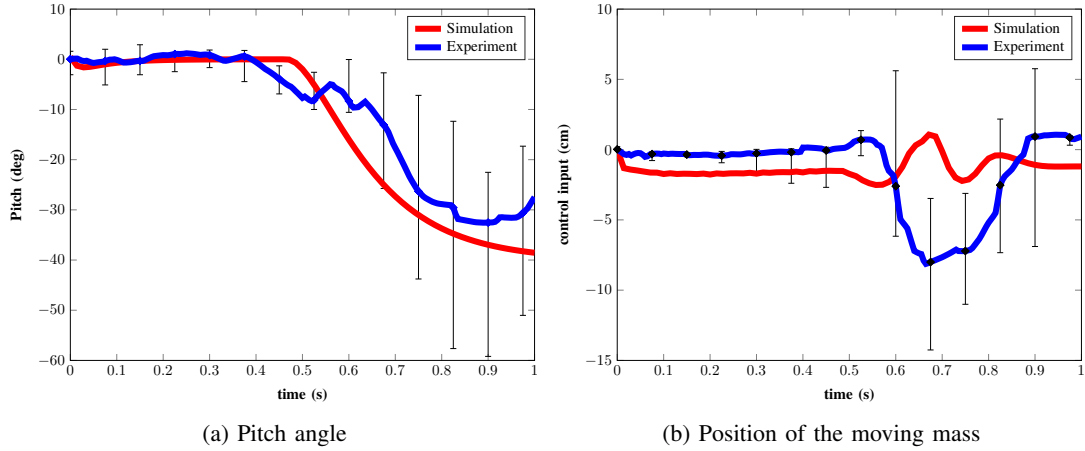


Fig. 6: A comparison of the simulated and experimental trajectories with  $40^\circ$  pitch up (negative) as a desired reference.

MAV was given an initial forward velocity at an approximate zero initial pitch angle. Results of two cases (tracking of  $5^\circ$  and  $40^\circ$  pitched up reference flights) are reported in this section. For each case, flight data for ten trials was recorded. Flight length was normalized to one second for comparison. Experimental data was post processed to determine statistical information of flight, the median, maximum and minimum flight trajectories. The state of the system is reported by on-board IMU. IMU reports angular position and velocity while linear velocities were synthesized by integrating the filtered accelerometer data. Accelerometer output was filtered using a low pass filter to remove sensor noise.

Experimental flight was compared to simulation for identical initial conditions. Fig. 5 (a) shows simulated and experimental pitch angle trajectories with  $5^\circ$  pitch up orientation as a desired reference. Here the experimental pitch angle trajectory is the median pitch angle trajectory determined from ten flight trials while the confidence bound associated with it is the maximum and minimum state limits from the ten flight trials. Fig. 5 (b) shows the control input, the position of the lump of mass. Similarly Fig. 6 shows tracking performance with  $40^\circ$  pitch up orientation as desired

reference. The current configuration employed for moving the lump of mass offers a limited distance that it can move in either direction. In order to achieve more maneuverability, a small mass was added behind CP to compensate for the actuator saturation. With CG behind CP in this configuration, the controller was able to track the reference trajectory. A comparison of control inputs for the two cases ( $5^\circ$  and  $40^\circ$  pitch angle), clearly supports that with a significant variation in the distance between CG and CP, any desired orientation can be achieved.

Fig. 7 shows *Allice* performing a high angle pitch up maneuver similar to the ones performed by bats while landing.

## VI. CONCLUSION

Bats perform a variety of maneuvers by virtue of high DOFs in their wings and their flexible membrane. Despite having high DOFs in wings, bats also regulate their CG-CP distance to perform maneuvers in the sagittal plane. In particular, they perform the landing maneuver by regulating the distance of their CG from their CP. This work is focused at recreating maneuvers that bats perform using a small MAV

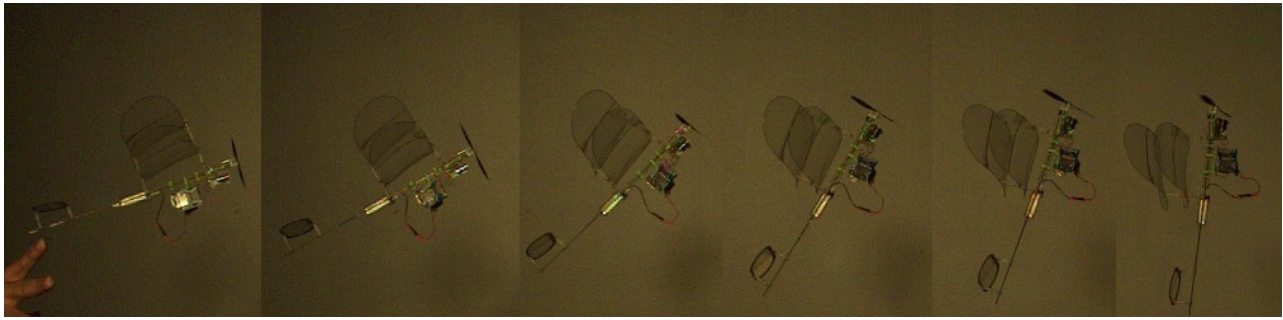


Fig. 7: *Alice* performing high angle pitch-up maneuver.

called *Alice*. CG-CP variation is materialized in *Alice* by moving a lump mass along its body  $x$ -axis which manipulates its pitch dynamics. A model based nonlinear control law using Input-Output Feedback Linearization is designed which enables tracking of the reference pitch trajectory. Simulation and experimental results validate the effectiveness of the CG-CP distance regulation for agile maneuverability.

#### REFERENCES

- [1] J. Yan, S. Avadhanula, J. Birch, M. Dickinson, M. Sitti, T. Su, and R. Fearing, "Wing transmission for a micromechanical flying insect," *Journal of Micromechanics*, vol. 1, no. 3, pp. 221–237, 2001.
- [2] J. E. Clark, J. G. Cham, S. A. Bailey, E. M. Froehlich, P. K. Nahata, R. J. Full, and M. R. Cutkosky, "Biomimetic design and fabrication of a hexapedal running robot," in *Robotics and Automation, 2001. Proceedings 2001 ICRA. IEEE International Conference on*, vol. 4, IEEE, 2001, pp. 3643–3649.
- [3] S.-J. Chung and M. Dorothy, "Neurobiologically inspired control of engineered flapping flight," *Journal of Guidance, Control, and Dynamics*, vol. 33, no. 2, pp. 440–453, 2010.
- [4] O. Unver, A. Uneri, A. Aydemir, and M. Sitti, "Geckobot: a gecko inspired climbing robot using elastomer adhesives," in *Proceedings 2006 IEEE International Conference on Robotics and Automation, 2006. ICRA 2006.*, May 2006, pp. 2329–2335.
- [5] A. Jusufi, D. T. Kawano, T. Libby, and R. J. Full, "Righting and turning in mid-air using appendage inertia: reptile tails, analytical models and bio-inspired robots," *Bioinspiration and Biomimetics*, vol. 5, no. 4, p. 045001, 2010.
- [6] D. K. Riskin, D. J. Willis, J. Iriarte-Díaz, T. L. Hedrick, M. Kostandov, J. Chen, D. H. Laidlaw, K. S. Breuer, and S. M. Swartz, "Quantifying the complexity of bat wing kinematics," *Journal of Theoretical Biology*, vol. 254, no. 3, pp. 604–615, 2008.
- [7] A. Ramezani, H. Vejdani, D. Boerma, S.-J. Chung, S. M. Swartz, K. S. Breuer, and S. Hutchinson, "From rousettus aegyptiacus landing to robotic landing: Synthesis and control of a reduced-order landing model," *submitted to IEEE International Conference on Robotics and Automation*, 2017.
- [8] A. Ramezani, X. Shi, S.-J. Chung, and S. Hutchinson, "Bat bot (b2), a biologically inspired flying machine," in *Proceedings of the IEEE International Conference on Robotics and Automation (ICRA)*, 2016.
- [9] —, "Lagrangian modeling and flight control of articulated-winged bat robot," *Proc. 2015 IEEE/RSJ International Conference on Intelligent Robots and Systems (IROS)*, Hamburg, Germany, September 28–October 02, 2015.
- [10] J. M. CAMHI, "Sensory control of abdomen posture in flying locusts," *Journal of Experimental Biology*, vol. 52, no. 3, pp. 533–537, 1970.
- [11] —, "Yaw-correcting postural changes in locusts," *Journal of Experimental Biology*, vol. 52, no. 3, pp. 519–531, 1970.
- [12] T. Libby, T. Y. Moore, E. Chang-Siu, D. Li, D. J. Cohen, A. Jusufi, and R. J. Full, "Tail-assisted pitch control in lizards, robots and dinosaurs," *Nature*, 2012.
- [13] E. Chang-Siu, T. Libby, M. Tomizuka, and R. J. Full, "A lizard-inspired active tail enables rapid maneuvers and dynamic stabilization in a terrestrial robot," in *2011 IEEE/RSJ International Conference on Intelligent Robots and Systems*, Sept 2011, pp. 1887–1894.
- [14] E. Chang-Siu, T. Libby, M. Brown, R. J. Full, and M. Tomizuka, "A nonlinear feedback controller for aerial self-righting by a tailed robot," in *Robotics and Automation (ICRA), 2013 IEEE International Conference on*, May 2013, pp. 32–39.
- [15] A. Jusufi, D. I. Goldman, S. Revzen, and R. J. Full, "Active tails enhance arboreal acrobatics in geckos," *Proceedings of the National Academy of Sciences*, vol. 105, no. 11, pp. 4215–4219, 2008.
- [16] Y. Laouris, J. Kalli-Laouri, and P. Schwartz, "The postnatal development of the air-righting reaction in albino rats. quantitative analysis of normal development and the effect of preventing neck-torso and torso-pelvis rotations," *Behavioural Brain Research*, vol. 37, no. 1, pp. 37–44, 1990.
- [17] T. Kane and M. Scher, "A dynamical explanation of the falling cat phenomenon," *International Journal of Solids and Structures*, vol. 5, no. 7, pp. 663–670, 1969.
- [18] J. P. Dyhr, K. A. Morgansen, T. L. Daniel, and N. J. Cowan, "Flexible strategies for flight control: an active role for the abdomen," *Journal of Experimental Biology*, vol. 216, no. 9, pp. 1523–1536, 2013.
- [19] J. M. ZANKER, "On the mechanism of speed and altitude control in drosophila melanogaster," *Physiological Entomology*, vol. 13, no. 3, pp. 351–361, 1988.
- [20] W. Wang, G. Song, K. Nonami, M. Hirata, and O. Miyazawa, "Autonomous control for micro-flying robot and small wireless helicopter x.r.b," in *2006 IEEE/RSJ International Conference on Intelligent Robots and Systems*, Oct 2006, pp. 2906–2911.
- [21] C. Bermes, S. Leutenegger, S. Bouabdallah, D. Schaefroth, and R. Siegwart, "New design of the steering mechanism for a mini coaxial helicopter," in *2008 IEEE/RSJ International Conference on Intelligent Robots and Systems*, Sept 2008, pp. 1236–1241.
- [22] I. C. Rust and H. H. Asada, "The eyeball rov: Design and control of a spherical underwater vehicle steered by an internal eccentric mass," in *Robotics and Automation (ICRA), 2011 IEEE International Conference on*. IEEE, 2011, pp. 5855–5862.
- [23] L. Jia-Wang, S. Bao-Wei, and S. Cheng, "Tracking control of autonomous underwater vehicles with internal moving mass," *Acta Automatica Sinica*, vol. 34, no. 10, pp. 1319–1323, 2008.
- [24] N. E. Leonard and J. G. Graver, "Model-based feedback control of autonomous underwater gliders," *Oceanic Engineering, IEEE Journal of*, vol. 26, no. 4, pp. 633–645, 2001.
- [25] C. A. Woolsey and N. E. Leonard, "Stabilizing underwater vehicle motion using internal rotors," *Automatica*, vol. 38, no. 12, pp. 2053–2062, 2002.
- [26] J. D. Anderson Jr, *Fundamentals of aerodynamics*. Tata McGraw-Hill Education, 2010.
- [27] M. W. Spong, S. Hutchinson, and M. Vidyasagar, *Robot modeling and control*. Wiley New York, 2006, vol. 3.
- [28] J. D. DeLaurier, "An aerodynamic model for flapping-wing flight," *The Aeronautical Journal (1968)*, vol. 97, no. 964, pp. 125–130, 07 2016.
- [29] R. F. Stengel, *Flight dynamics*. Princeton University Press, 2015.
- [30] M. P. Miller, "An accurate method of measuring the moments of inertia of airplanes," 1930.
- [31] N. Hovakimyan, E. Lavretsky, and C. Cao, "Dynamic inversion for multivariable non-affine-in-control systems via time-scale separation," *International Journal of Control*, vol. 81, no. 12, pp. 1960–1967, 2008.
- [32] H. K. Khalil and J. Grizzle, *Nonlinear systems*. Prentice hall New Jersey, 1996, vol. 3.